Terahertz coherent radiation from steady-state microbunching in storage rings with *X*-band radio-frequency system

Yi Jiao, Daniel F. Ratner, and Alexander W. Chao

SLAC National Accelerator Laboratory, Menlo Park, California, 94025, USA
(Received 20 July 2011; published 18 November 2011)

The mechanism of steady-state microbunching (SSMB) has been proposed [D. F. Ratner and A. W. Chao, Phys. Rev. Lett. **105**, 154801 (2010)] to produce steady-state microbunched beams by using laser modulations in a storage ring for generating coherent radiation with high repetition rate at wavelengths from the submillimeter to extreme ultraviolet range. In the present paper, we analyze the dynamics of the SSMB system with a Hamiltonian and Jacobi matrix approach and identify the original proposal of SSMB as a mechanism with period-1 fixed point in phase space. We then propose an alternative SSMB mechanism with period-2 fixed point, which is able to produce microbunched beams with shorter bunch length and, hence, higher harmonic. Taking the SPEAR3 storage ring as an example, we illustrate the application of the period-2 SSMB to generate terahertz (THz) steady-state coherent radiation in a storage ring using an *X*-band radio-frequency (rf) system instead of a more technically demanding laser system. Issues covered include choice of rf parameters, system errors, beam lifetime, collective effects, and radiation power evaluation. Compared to the more traditional low-momentum-compaction operation mode, the proposed SSMB scheme potentially promises higher beam current, larger bunching factor, and hence brightness increase of at least 1 order of magnitude.

I. INTRODUCTION

High peak brilliance and high repetition rate are both of significant importance for light sources. Linac driven free electron laser (FEL) facilities usually have extremely high brilliance because their beam is highly microbunched during the FEL process, but have low repetition rate (see, e.g. [1]). On the other hand, storage ring-based light sources, typically the third generation light sources, have high repetition rate due to intrinsic rapid beam circulation, but have relatively low brilliance because storage rings generally do not support microbunched beams.

Past schemes have proposed generating beams with both high repetition rate and high brilliance. For example, Kim, Shvydko, and Reiche proposed to use a cw superconducting linac to increase the FEL pulse repetition rate up to MHz [2]. Energy recovery linacs also promise high repetition rate [3,4]. Storage ring FELs were proposed to generate coherent, monochromatic radiations in storage rings (see, e.g. [5]). Recently, Ratner and Chao [6] proposed steady-state microbunching (SSMB) to establish a beam that has a fixed microbunching structure turn after turn at the location of a radiator in a storage ring to generate coherent radiation at a high repetition rate or in continuous wave mode. They illustrate the basic mechanism of the SSMB as follows.

Consider a sine modulation $V\sin(2\pi z/\lambda_{\mathrm{mod}})$ of a beam in a storage ring. A particle with specific nonzero relative momentum deviation δ_0 and $z_0 = 0$ has a longitudinal displacement $\Delta z = R_{56}\delta_0$ after one turn, where $R_{56} = \alpha C$ is the longitudinal dispersion with α the momentum compaction and C the circumference of the storage ring. If $\Delta z = \lambda_{\mathrm{mod}}$, the particle does not return to its initial position but moves to an equivalent zero crossing $[\sin(2\pi\Delta z/\lambda_{\mathrm{mod}}) = 0]$ turn after turn due to the modulation's periodicity. The points $(0, n\delta_0)$, with $n = 0, \pm 1, \pm 2$, etc., are considered to be single turn (period-1) fixed points (modulus λ_{mod}). Thus, at each zero crossing, there will be a set of fixed points in phase space. After a fraction, $1/H$, of a turn instead of a full turn, the fixed points and the particles around the fixed points will have different longitudinal displacements in phase space, $n\lambda_{\mathrm{mod}}/H$. Consequently, strong microbunching is obtained with a period of λ_{mod}/H. By placing a radiator (dipole or wiggler) at this position, SSMB generates high repetition rate, coherent radiation of wavelength $\lambda_{\mathrm{r}} = \lambda_{\mathrm{mod}}/H$. To maintain particles around H fixed points within one modulation wavelength, it requires large enough momentum aperture A_δ and/or short modulation wavelength, $A_\delta \sim H\delta_0/2 = H\lambda_{\mathrm{mod}}/2\alpha C$. As illustrated in Ref. [6], period-1 SSMB with laser modulations potentially promises high harmonic number. Because the laser modulation wavelength is typically small, the momentum aperture constraint is easily satisfied; taking the SPEAR3 storage ring [7] as example, $C = 234.126$ m, $A_\delta = 0.03$, and $\alpha = 0.0011$ for regular user operation mode, with a laser source of wavelength $\lambda_{\mathrm{mod}} = 1$ μm, the momentum aperture is orders of magnitude larger than the energy spacing δ_0.

In the case that the momentum aperture is small and/or modulation wavelength is long (e.g., rf modulation), one can to some extent mitigate the limitation on the available harmonic number by applying modulations once every multiple turns (however, the modulation interval cannot be too large, otherwise the longitudinal wakefield and other effects will cause the microbunching structure to smear in phase space) and therefore increase the equivalent α of the SSMB system. Moreover, based on the fact that the coherent radiation wavelength highly depends on the separation of the density peaks rather than the evenly distributed structure, one can still generate high harmonic coherent radiation even with a few microbunches (see Fig. 1).

In the above discussion, the microbunched beam is assumed to have vanishing bunch length. However, the equilibrium rms bunch length (Gaussian distribution) σ_z due to the radiation damping and quantum excitation in a storage ring is not arbitrarily small. In reality, the available harmonic number is usually limited by the bunch length. It requires

$$H \le \frac{\lambda_{\mathrm{mod}}}{2\sqrt{2\ln2}\,\sigma_z}. \qquad (1.1)$$

Otherwise the density peaks will overlap each other and destroy the expected microbunching structure at λ_{mod}/H. Thus, the key point for high harmonic SSMB is to minimize the length of the microbunched beam. A typical two-stage modulation system was analyzed in Ref. [6] using linearized one-turn map and generalized longitudinal Courant-Snyder parameters. It is found that using strong modulations [normalized amplitude $|K| \lesssim 4$, K is defined by Eq. (2.2) below], the bunch length can be significantly
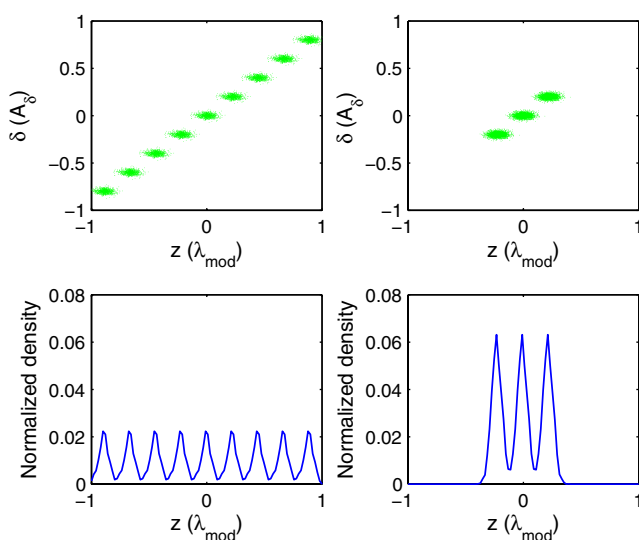

FIG. 1. Period-1 SSMB with $H = 9$, left figures show evenly distributed microbunches within one modulation wavelength, and right figures show three microbunches with separation of λ_{mod}/H. Both cases generate coherent radiation of wavelength $\lambda_r = \lambda_{\mathrm{mod}}/H$.

reduced (see [8–12] for other methods for short bunches). However, the linearized model becomes invalid for strong modulations, in which case the nonlinearity arisen from the sine function dominates the dynamics of the SSMB system. We therefore look into the detailed dynamics of such a system using a Hamiltonian and Jacobi matrix approach in this paper. Our study shows that with slightly stronger modulations ($|K| \gtrsim 4$), period-1 fixed points become unstable, however, period-2 fixed points emerge, repeating themselves (modulus λ_{mod}) every two turns in phase space. Based on the analysis, we propose a period-2 SSMB mechanism, i.e., SSMB based on period-2 fixed points, which doubles the number of the microbunches, and promises much smaller bunch length and thus potentially higher harmonic than period-1 SSMB. Even in the case that only conventional buckets are allowed in phase space ($A_\delta < \lambda_{\mathrm{mod}}/\alpha C$), period-2 SSMB can produce two microbunches and, hence, two density peaks with tunable spacing within one modulation wavelength. Thus, this proposed SSMB can be established using a rf system with relatively long wavelength, e.g., to generate THz coherent radiation in a storage ring using an X-band rf cavity instead of a more technically demanding laser beating technique which uses two laser sources with a small difference in wavelengths [6,13]. Compared with the traditional THz light source working with low momentum compaction (see [14] and the references therein), period-2 SSMB reduces the bunch length by increasing the modulation amplitude, and operates with momentum compaction on the same order of magnitude as that of regular user operation mode. It therefore allows a relatively large longitudinal tune and promises high average beam current in a storage ring. (Strong focusing was proposed to improve the traditional THz light source, see e.g. [15,16], in which, however, the bunch length is mainly reduced by decreasing the momentum compaction.) Because the coherent radiation power is proportional to the square of the stored beam current, with period-2 SSMB scheme, one can expect an enhancement of brightness of at least 1 order of magnitude compared to the traditional THz light source.

In Sec. II A, we present the Hamiltonian of the SSMB system and view the variation of the dynamics with modulation amplitude K, from which we reidentify the condition for period-1 SSMB that was studied in Ref. [6] and extend the parameter range to include period-2 fixed points. An alternative SSMB mechanism based on period-2 fixed points is then proposed. Subsequently, the fixed points, local instability condition, and synchrotron tune of the motions around the fixed points are investigated with the Jacobi matrix in Sec. II B. The relative area and relative length of the stable islands around the period-1 and period-2 fixed points are derived in Sec. II C. The numerical results confirm the analytical predictions. In Sec. II D, the dynamics of the SSMB system including the effects of radiation damping and quantum excitation is discussed.

Taking the SPEAR3 storage ring as an example, we illustrate the application of the proposed period-2 SSMB using an X-band rf cavity. In Sec. III A, we discuss the requirements for the X-band rf system, and then implement numerical simulations, including the radiation damping, quantum excitation effects, and random errors, to verify the parameter choice. Collective effects, such as coherent synchrotron radiation (CSR) wakefield, X-band longitudinal short range wakefield, and heating from the interaction of beam with small discontinuities of the storage ring, are evaluated in Sec. III B. It appears there is no insurmountable difficulty for a proof-of-principle experiment of period-2 SSMB in the SPEAR3 storage ring. The steady-state THz coherent radiation power produced by the proposed SSMB scheme is calculated in Sec. III C. Discussion on further improving the coherent radiation power is present in Sec. III D. Conclusions are given in Sec. IV.

II. SSMB SYSTEM DYNAMICS

The steady-state microbunch length sets the highest achievable harmonic according to Eq. (1.1). In general, the microbunch length is determined by the smaller of the stable island size (set by the Hamiltonian of the modulation and dispersion) and the equilibrium bunch length (set by the radiation damping and quantum excitation in a ring). Reference [6] used a linearized analysis to study the two-stage modulation SSMB mechanism. To provide a more complete picture of the dynamics, we have studied both one-stage and two-stage modulation systems using a Hamiltonian and Jacobi matrix approach. This more complete approach illustrates the transition from period-1 to period-2 SSMB, and allows us to calculate the phase space dimensions of the stable islands. In this section, we first use Hamiltonian and Jacobi matrix methods to study the stable islands, and then compare the results to the equilibrium island length due to radiation damping and quantum excitation. For brevity, we only present the analysis of the one-stage modulation system here. Extension to two-stage modulation system is straightforward.

A. Hamiltonian of SSMB system

The SSMB system with one-stage modulation can be described as

$$z_1 = z_0, \qquad \delta_1 = \delta_0 + V\sin(kz_0),$$
$$z_2 = z_1 + R_{56}\delta_1, \qquad \delta_2 = \delta_1, \tag{2.1}$$

where z and δ are the longitudinal displacement and relative momentum deviation of a particle relative to the synchronous particle, respectively. Each particle experiences a modulation kick, $V\sin(kz)$ with $V = \mathrm{eV_{mod}}/E_0$ (E_0 is the nominal beam energy, V_{mod} is the modulation voltage) and $k = 2\pi/\lambda_{mod}$, and then passes through a longitudinal dispersive region before it returns to the modulation source.

It is convenient to transform the variables z, δ, and V to dimensionless quantities,

$$\theta = kz, \qquad I = R_{56}k\delta, \qquad K = VR_{56}k. \tag{2.2}$$

Accordingly, Eq. (2.1) becomes

$$I_1 = I_0 + K\sin\theta_0, \qquad \theta_1 = \theta_0 + I_1, \tag{2.3}$$

where I and θ are both periodic in 2π.

Note that Eq. (2.3) is the well-known "standard map" (see, e.g. [17]), whose Hamiltonian dynamics has been systematically studied by Chirikov with regard to chaotic phenomena from the sine nonlinearity. In what follows, we summarize the variation of the SSMB system dynamics with the modulation amplitude K, and concentrate on the condition of small stable island length which is closely related to the available SSMB harmonic.

Following Ref. [17], Eq. (2.3) can be described with the pendulum Hamiltonian driven by a periodic perturbation,

$$H(J, \theta, t) = \frac{1}{2}J^2 + \kappa \sum_{n=-\infty}^{\infty} \cos(\theta - nt), \tag{2.4}$$

where $J = I/2\pi$ and $\kappa = K/4\pi^2$.

With the method of canonical perturbation analysis [17,18], one can derive the location J_r and island height (ΔJ) of the resonances.

Integer resonance

$$(J_r)_1 = n, \qquad (\Delta J)_1 = 2\sqrt{\kappa} = \sqrt{K}/\pi. \tag{2.5}$$

Half integer resonance

$$(J_r)_2 = (2p + 1)/2, \qquad (\Delta J)_2 = \pi\kappa. \tag{2.6}$$

Third order resonance

$$(J_r)_3 = q/3, \qquad (\Delta J)_3 = 9.3\kappa^{3/2}. \tag{2.7}$$

In Eqs. (2.5), (2.6), and (2.7), n, p, q are arbitrary integers.

The resonance island heights depend on $\kappa = K/4\pi^2$ and increase with increasing K. Once the separatrices of two adjacent resonances overlap each other, the frequency of the motion in the overlapping region will jump randomly from one resonance to the other; therefore the motion loses periodicity and becomes chaotic or stochastic [16]. As a straightforward inference, if the center (fixed point) of one resonance island touches the separatrix of the adjacent resonance, all the motions inside this resonance island will be irregular and the stable island will disappear in phase space. For example, the condition for the half integer resonance island disappearing can be estimated by

$$(\Delta J)_1 = \tfrac{1}{2}, \qquad \text{or} \qquad (\Delta J)_3 = \tfrac{1}{6}, \tag{2.8}$$

which yields $K = 2.46$ or 2.70, not far from the obtained critical value $K \approx 2.2$ from numerical simulations for the disappearance of the half integer resonance island.

We simulate the motions described by Eq. (2.3) for different positive K values (the dynamics is the same for
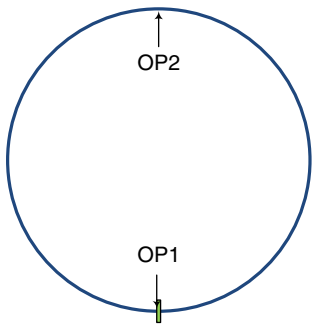
FIG. 2.   One-stage modulation SSMB system. The green box indicates the modulation source. OP1 and OP2 indicate the observation points at the entrance and the opposite of the modulation source, respectively.

negative K, only with the fixed points changed in phase space, see Sec. II B), with geometry shown in Fig. 2 and particle coordinates in phase space of (θ, I) at the entrance of the modulation source shown in Fig. 3. For $0 < K < 1$, the motions are regular and the resonance islands are stable. The central integer resonance islands $[(J_r)_1 = 0]$ correspond to conventional buckets in a storage ring provided the modulation source is an rf cavity. At K around 1, stochastic motions emerge neighboring the separatrices of the resonances. As K increases, the stable islands will shrink or even disappear due to resonance overlapping. For $3 < K < 4$, only integer resonance islands remain stable. Of particular interest are the cases with $4 < K < 2\pi$. Each integer resonance island splits into two islands (around period-2 fixed points) with much smaller length. When K is close to 2π, the stable island size will tend to zero (very small but not zero). When $K > 2\pi$, the coordinate I (or δ) will increase continuously each turn, corresponding to particle loss in a storage ring with a finite momentum aperture.

The islands will rotate in phase space when particles pass through a dispersive section. Assuming R_{56} varies monotonically along the ring, for a given K, the island length reaches its minimum on the opposite of the modulation source (OP2 in Fig. 2), as shown in Fig. 4 with cases of $K = 3.5$ and 5 as examples. The fixed points of the integer resonance islands change to $(\theta_0 - I_0/2, I_0)$ in phase space.

From the above analysis, we learn that, the modulation amplitude should be large enough, e.g. $|K| \geq 3$, so that one can obtain clear stable island structure in phase space and, hence, clear density modulation at the radiator; the stable integer resonance island length reaches its minimum when K is below and close to 4; finally, with $|K|$ slightly larger than 4, motions around period-1 fixed points are unstable, but they bifurcate into stable islands around period-2 fixed points with islands number doubled and much smaller island length compared to that around period-1 fixed points. Combining conditions (1.1), with a slightly stronger modulation than that required by period-1 SSMB, the SSMB based on period-2 fixed points is capable of

generating shorter microbunched beams associated with higher harmonic compared to period-1 SSMB. Even in the case that the modulation source is a rf system with relatively long wavelength and only conventional buckets $[(J_r)_1 = 0]$ are allowed by the momentum aperture, one can still produce two short microbunches with different energy deviations using a strong modulation ($|K| \gtrsim 4$); with an optimal R_{56} between the modulation source and the radiator, one can obtain a sharply double-peaked longitudinal density distribution at the radiator, which helps generate coherent radiation at a wavelength equal to the separation between the two density peaks.

It should be mentioned that there exist period-3 or even higher-order periodic fixed points and stable islands [17,19]. However, the corresponding stable islands have such small size that they have little practical value. Thus, here we concentrate only on the period-1 and period-2 trajectories and stable islands.

B. Period-1 and period-2 fixed points

Based on the Hamiltonian dynamics of the SSMB system, we derive the stability condition and the synchrotron tune of the motion around period-1 and period-2 fixed points.

For the single turn map, Eq. (2.3), the period-1 fixed points are determined by

$$\Delta I = I_1 - I_0 = 0, \qquad \Delta\theta = \theta_1 - \theta_0 = 0(\text{mod}2\pi), \quad (2.9)$$

which results in $(\theta_0, I_0) = (\pi n, 2\pi n)$, $n = 0, \pm 1, \pm 2$, etc.

Let us consider the particle motion with initial condition $(\theta_0 + \delta\theta, I_0 + \delta I)$. From Eq. (2.3), one can obtain a linearized map,

$$\begin{pmatrix} \delta\theta \\ \delta I \end{pmatrix}_1 = \begin{pmatrix} 1 + K\cos\theta_0 & 1 \\ K\cos\theta_0 & 1 \end{pmatrix} \begin{pmatrix} \delta\theta \\ \delta I \end{pmatrix}_0 = M_1 \begin{pmatrix} \delta\theta \\ \delta I \end{pmatrix}_0, \quad (2.10)$$

where M_1 is the period-1 Jacobi matrix.

The synchrotron tune of the motion around a period-1 fixed point is given by

$$\cos(\nu_s) = \tfrac{1}{2}\text{Tr}M_1 = 1 + K\cos\theta_0/2. \quad (2.11)$$

To keep the motion bounded, it requires $|\text{Tr}M_1| < 2$, which results in

$$-4 < K\cos\theta_0 < 0. \quad (2.12)$$

From Eqs. (2.9) and (2.12), the period-1 fixed points are $(0, 0)$ (mod 2π) for $-4 < K < 0$, and $(\pi, 0)$ (mod 2π) for $0 < K < 4$.

To study the period-2 fixed points, we write the map of two iterations of the one-stage modulation system as

$$I_1 = I_0 + K\sin\theta_0, \qquad \theta_1 = \theta_0 + I_1,$$
$$I_2 = I_1 + K\sin\theta_1, \qquad \theta_2 = \theta_1 + I_2. \quad (2.13)$$
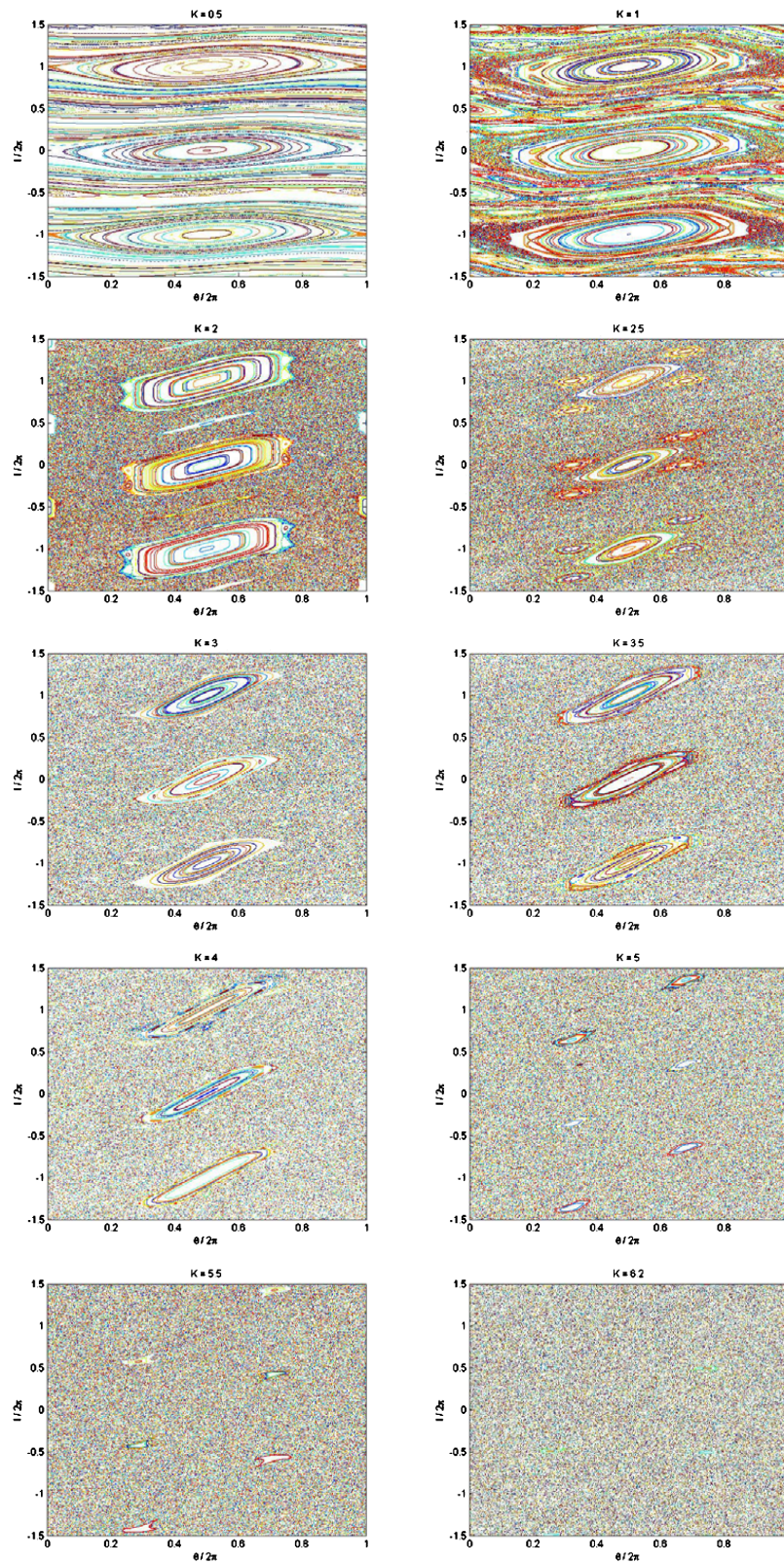
FIG. 3.   The motions described by Eq. (2.3) in phase space with $K = 0.5$, 1, 2, 2.5, 3, 3.5, 4, 5, 5.5, and 6.2, and with observation point at the entrance of the modulation (OP1 in Fig. 2).
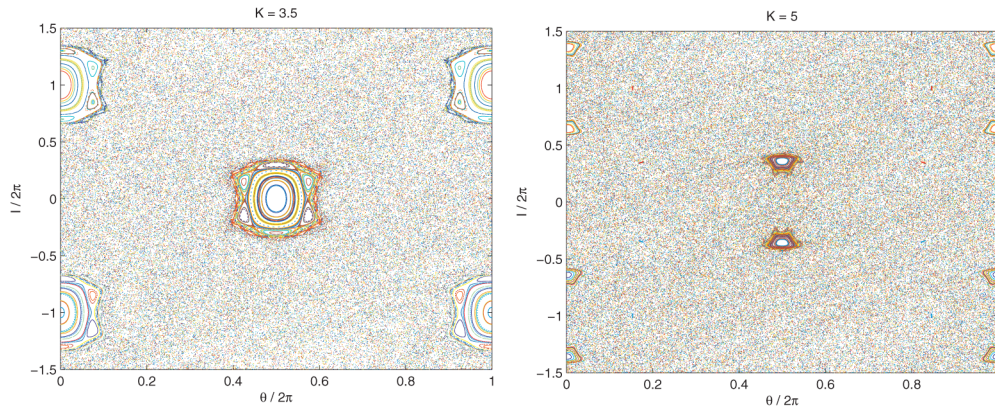
FIG. 4.   The motions described by Eq. (2.3) in phase space with $K = 3.5$ and 5, and with observation point on the opposite of the modulation (OP2 in Fig. 2).

The period-2 fixed points are determined by

$$\Delta I = I_2 - I_0 = K(\sin\theta_1 + \sin\theta_0) = 0,$$

$$\Delta\theta = \theta_2 - \theta_0 = I_2 + I_1 = 0(\mathrm{mod}2\pi). \quad (2.14)$$

There are two solutions for Eq. (2.14), $\theta_0 + \theta_1 = 0$ (mod 2π) or $\theta_0 - \theta_1 = \pi$ (mod 2π). However, only the first solution is available in practice, corresponding to $K\cos\theta_0 = K\cos\theta_1$. By combining Eqs. (2.13) and (2.14), we obtain

$$I_2 - I_1 = 2I_2(\mathrm{mod}\,2\pi) = K\sin\theta_1,$$
$$\theta_2 - \theta_1 = -2\theta_1(\mathrm{mod}\,2\pi) = I_2, \quad (2.15)$$

from which we have

$$4\theta_1 + K\sin\theta_1 = 2\pi n. \quad (2.16)$$

One can numerically solve Eq. (2.16) to obtain θ_1, and then calculate θ_0, I_0, I_1 from Eq. (2.15).

The period-2 Jacobi matrix can be derived from Eq. (2.13),

$$M_2 = \begin{pmatrix} 1 + K\cos\theta_1 & 1 \\ K\cos\theta_1 & 1 \end{pmatrix}\begin{pmatrix} 1 + K\cos\theta_0 & 1 \\ K\cos\theta_0 & 1 \end{pmatrix}. \quad (2.17)$$

With the known condition $K\cos\theta_0 = K\cos\theta_1$, we obtain the expression of the synchrotron tune and the stability condition,

$$\cos(2\nu_s) = 1 + 2K\cos\theta_1 + K^2\cos^2\theta_1/2,$$
$$-4 < K\cos\theta_1 < 0, \quad (2.18)$$

where ν_s is the equivalent "one-turn" synchrotron tune of the motion around period-2 fixed points.

From the stability condition, we can approximate $\theta_1 = \theta_{10} + \delta\theta_{10}$ with $\theta_{10} = \cos^{-1}(-2/K)$ (mod 2π) and $\delta\theta_{10} \ll \theta_{10}$. Using Eq. (2.16), we obtain an approximate expression of θ_1 to the first order of $\delta\theta_{10}$,

$$\theta_1 = \pi - \sqrt{K^2 - 4}/2 + \cos^{-1}(2/K)(\mathrm{mod}\,2\pi). \quad (2.19)$$

Figure 5 shows the synchrotron tune ν_s and fixed point θ_0 (or θ_1) of the SSMB system with the modulation amplitude K ranging from 0 to 2π. The longitudinal tunes with $0 < K < 4$ and $4 < K < 2\pi$ correspond to that of the motions around period-1 and period-2 fixed points, respectively. So they are not continuous at $K = 4$. The accuracy of Eq. (2.19) degrades when K is close to 4 or 2π, in which cases the assumption $\delta\theta_{10} \ll \theta_{10}$ is not well satisfied.

C. Period-1 and period-2 stable islands

As mentioned, along with increasing modulation amplitude K, the stable resonance islands will shrink due to resonance overlapping. In this section, we derive the relative stable island area S and relative stable island length R for the two cases of interest. The first case is when only integer resonance islands are stable in phase space ($3 < K < 4$) and the second case is when each integer
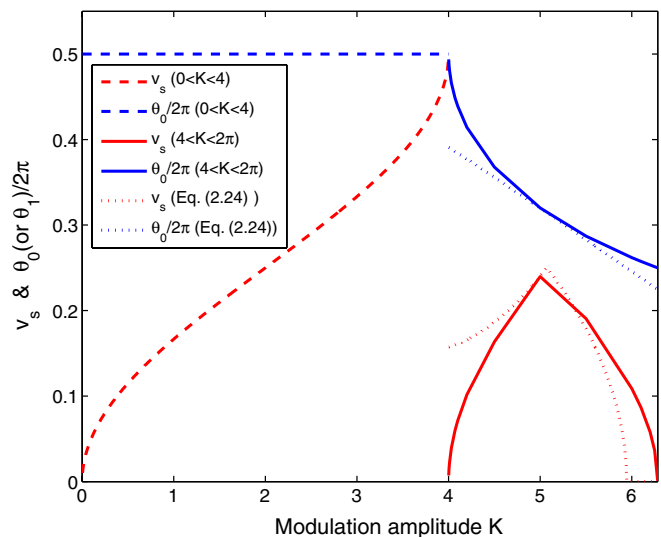

FIG. 5.   Variation of ν_s and θ_0 (or θ_1) with respect to modulation amplitude K.
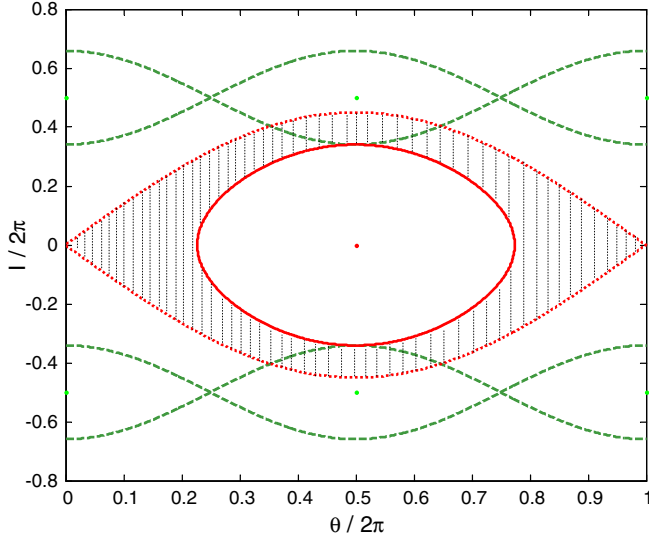
FIG. 6. Shrinkage of the stable integer resonance island due to resonance overlapping between the adjacent integer and half integer resonance islands. The green dashed lines and red dotted lines indicate the separatrices of the half integer and integer resonance islands in a single resonance approach, respectively. The red solid line indicates the boundary of the integer resonance island stable area.

resonance island splits into two smaller islands ($4 < K < 2\pi$). Assuming the initial particles are uniformly distributed in phase space and there is not any damping mechanism, S and R are closely related to the percentage of the surviving particles and available bunch length.

For $3 < K < 4$, we consider the resonance overlapping between the integer and half integer resonance islands, assuming the islands are upright in phase space (see Fig. 6). For a given K, the maximum J of the half integer resonance island is

$$(\Delta J)_2 = \pi\kappa = \frac{K}{4\pi}. \tag{2.20}$$

Because of resonance overlapping, the maximum height (with $\theta = \pi$) of the stable integer resonance island is

$$J_{1,\max} = \frac{1}{2} - (\Delta J)_2 = \frac{1}{2} - \frac{K}{4\pi}. \tag{2.21}$$

Using the Hamiltonian of the integer resonance $J_r = 0$ (with positive K)

$$H(J,\theta) = \frac{1}{2}J^2 + \kappa\cos(\theta) = \frac{1}{2}J^2 - \frac{K}{4\pi^2}\cos(\theta - \pi), \tag{2.22}$$

and $J = J_{1,\max}$, $\theta = \pi$, we obtain the Hamiltonian of the motion at the boundary of the stable area,

$$H_b = \frac{1}{2}\left(\frac{1}{2} - \frac{K}{4\pi}\right)^2 - \frac{K}{4\pi^2}. \tag{2.23}$$

From Eq. (2.22), θ arrives at the farthest point from π when J tends to 0, i.e. $\Delta\theta = \theta - \pi$ reaches the maximum value,

$$H_b = 0 - \frac{K}{4\pi^2}\cos(\Delta\theta_{\max}). \tag{2.24}$$

By combining Eqs. (2.23) and (2.24), we obtain $\Delta\theta_{\max}$ to the first order,

$$\Delta\theta_{\max} \approx \frac{\pi - K/2}{\sqrt{K}}. \tag{2.25}$$

In the range of $-1/2 < J < 1/2$ and $0 < \theta < 2\pi$, there exists only one stable integer resonance island. The relative length R and relative beam area S can be estimated by

$$R = \frac{2\Delta\theta_{\max}}{2\pi} \approx \frac{\pi - K/2}{\pi\sqrt{K}}, \tag{2.26}$$

$$S \approx \frac{\pi \times \Delta\theta_{\max} \times J_{1,\max}}{2\pi} \approx \frac{(\pi - K/2)^2}{4\pi\sqrt{K}}, \tag{2.27}$$

where S is obtained assuming the stable island is in the shape of an ellipse with major and minor radii of $\Delta\theta_{\max}$ and $\Delta J_{\max}$. Note that S is approximately proportional to R^2. Thus, to achieve a small relative bunch length, one has to pay with a larger particle loss rate.

Now consider one of the islands around the period-2 fixed point for $4 < K < 2\pi$ (see, e.g., the middle left island for the $K = 5$ case in Fig. 2). For simplicity, the fixed point is approximated by $\theta_{10} = \cos^{-1}(-2/K)$ and $J_{10} = -(K^2 - 4)^{1/2}/4\pi$.

The θ is limited by the stability condition in Eq. (2.18), therefore the minimum and maximum θ of the island boundary are given by

$$\theta_{11} = \pi/2, \qquad \theta_{12} = \cos^{-1}(-4/K). \tag{2.28}$$

Then the relative length R of the stable island is obtained:

$$R = \frac{\cos^{-1}(-4/K) - \pi/2}{2\pi}. \tag{2.29}$$

We write the Hamiltonian at the island boundary as

$$\begin{aligned}
H_b &= \frac{1}{2}J_{11}^2 + \frac{K}{4\pi^2}\cos\theta_{11} = \frac{1}{2}(J_{10} + \Delta J_{11})^2 \\
&= \frac{1}{2}J_{12}^2 + \frac{K}{4\pi^2}\cos\theta_{12} = \frac{1}{2}(J_{10} + \Delta J_{12})^2 - \frac{1}{\pi^2},
\end{aligned} \tag{2.30}$$

where J_{11}, J_{12} are the action coordinates conjugate to θ_{11} and θ_{12} and $\Delta J_{11} = J_{11} - J_{10}$, $\Delta J_{12} = J_{12} - J_{10}$, are assumed to be much smaller than J_{10}. We obtain

$$J_{21} = \Delta J_{12} - \Delta J_{11} \approx \frac{1}{\pi^2 J_{10}}, \tag{2.31}$$

and then estimate J_{11} by

$$J_{11} \approx J_{10} - J_{21} \times \frac{\cos^{-1}(-2/K) - \pi/2}{\cos^{-1}(-4/K) - \pi/2}. \tag{2.32}$$

With the known J_{11} and θ_{11}, we can evaluate the $J = J_{10} + \Delta J$ with $\theta = \theta_{10}$ at the island boundary using the Hamiltonian,

$$
\begin{aligned}
H_b &= \frac{1}{2}J_{11}^2 + \frac{K}{4\pi^2}\cos\theta_{11} = \frac{1}{2}J_{11}^2 \\
&= \frac{1}{2}(J_{10} + \Delta J)^2 + \frac{K}{4\pi^2}\cos\theta_{10} \\
&\approx \frac{1}{2}(J_{10} + \Delta J)^2 - \frac{1}{2\pi^2},
\end{aligned}
\tag{2.33}
$$

which yields

$$
\Delta J \approx \sqrt{J_{11} + \frac{1}{\pi^2}} - J_{10}.
\tag{2.34}
$$

Note that the island is tilted in phase space, approximately in the shape of an ellipse with major radius approximately of $\Delta\theta = (\theta_{12} - \theta_{11})/2$ and minor radius of ΔJ. Then the relative area S of the stable islands (there are two such islands in the range of $-1/2 < J < 1/2$ and $0 < \theta < 2\pi$) can be estimated by

$$
S \approx \frac{2 \times \pi \times \Delta J \times \Delta\theta}{2\pi} = \Delta J \times \Delta\theta.
\tag{2.35}
$$

Table I lists the R and S from analytical formulas and numerical measurements. Considering the rather rough single resonance assumption used in the derivation, the agreement between the two approaches is fairly good, especially for the relative stable island area S.

For the cases shown in Fig. 4, the relative stable island area S is the same as that in Table I, and the relative island length can be derived from a modified map and the corresponding Hamiltonian. The analytical results are $R = 0.33$ for $K = 3$ and $R = 0.054$ for $K = 5$, while the numerical results are $R = 0.2$ for $K = 3$ and $R = 0.08$ for $K = 5$.

Provided the momentum aperture is large enough, the available maximum harmonic $H_{\max}$ is determined by

$$
H_{\max} = N\left(\frac{1}{R}\right),
\tag{2.36}
$$

where $N(x)$ gives the largest integer not greater than x.

TABLE I.   Comparison of analytical predictions with the numerical measurements.

K	$S_{\text{analytical}}$	$R_{\text{analytical}}$	$S_{\text{numerical}}$[a]	$R_{\text{numerical}}$
6.28	0.0042	0.1099	0.0025	0.065
6.21	0.0045	0.1113	0.004	0.065
5	0.016	0.1476	0.014	0.12
4	0.084	0.25	0.08	0.40
3	0.124	0.30	0.11	0.43

[a]The values for the relative stable island area are obtained by Chirikov through precise numerical measurements (see Table 5.3 in Ref. [17]).

D. Effects of radiation damping and quantum excitation

Up to this point, we have obtained the relative island phase space dimensions (height, width, and area) using the Hamiltonian in the absence of radiation damping and quantum excitation effects. In an actual ring, the island phase space dimensions indicate the boundary of the stable motion area, while the rms bunch length and energy spread are determined by the equilibrium of radiation damping and quantum excitation effects. The rms bunch length determines the harmonic limit, so at this point we study the damping and excitation effects.

Let us consider the case that the SSMB system has one modulation source and R_{56} varies monotonically along the ring. In the dispersive region, the rms energy spread σ_δ is constant, and estimated by

$$
\sigma_\delta = \gamma\sqrt{\frac{C_q}{J_\varepsilon\rho}},
\tag{2.37}
$$

where $C_q = 3.832 \times 10^{-13}$ m, γ is the Lorentz factor, $J_\varepsilon \approx 2$ is the longitudinal damping partition number, and ρ is the radius of circular orbit.

From the Jacobi matrix (with variables of θ and I), we derive the rms bunch length σ_z,

$$
\sigma_z = \sqrt{\frac{\beta_0 - 2s\alpha_0 + \gamma_0 s^2}{\gamma_0}} R_{56}\sigma_\delta,
\tag{2.38}
$$

with the generalized longitudinal Courant-Snyder parameters at the exit of the modulation source in the form

$$
\beta_0 = \frac{1}{\sin(2\pi\nu_s)}, \qquad \alpha_0 = \frac{-K\cos[\theta_0(\text{or }\theta_1)]}{2\sin(2\pi\nu_s)},
$$

$$
\gamma_0 \equiv \frac{1 + \alpha_0^2}{\beta_0} = \frac{-K\cos[\theta_0(\text{or }\theta_1)]}{\sin(2\pi\nu_s)},
$$

where ν_s is determined by Eq. (2.11) or (2.18) and $0 < s < 1$.

At $s = 1/2$, the bunch length reaches its minimum,

$$
\sigma_{z,\min} = R_{56}\sigma_\delta\sqrt{\frac{-1}{K\cos[\theta_0(\text{or }\theta_1)]} - \frac{1}{4}}.
\tag{2.39}
$$

In a storage ring, there always is a rf system for injection, trapping particles and providing energy loss (due to synchrotron radiation) compensation, with much smaller normalized amplitude K and much larger bucket (or stable island) than that of the modulation source in a SSMB scheme. As we know, if with only the original rf system, the quantum lifetime is determined by

$$
\tau_q = \frac{1}{2}\tau_z \frac{e^{A_\delta^2/2\sigma_\delta^2}}{(A_\delta^2/2\sigma_\delta^2)},
\tag{2.40}
$$

where τ_z is the longitudinal damping time, and the overall momentum aperture A_δ is determined by the existing rf system with long buckets and transverse dynamics.

In order to obtain a long enough quantum lifetime, i.e., several hours, it requires $A_\delta > 6\sigma_\delta$.

However, the condition would be slightly changed when introducing strong modulation into the ring. Small islands are formed within the overall momentum aperture by the strong modulation, with island height of A_{island}. If $A_{\text{island}} > 6\sigma_\delta$, the vast majority of the microbunched particles will stay inside the small islands, and thus we obtain a long quantum lifetime. (In this case, the Touschek lifetime is usually long enough.) If $3\sigma_\delta < A_{\text{island}} < 6\sigma_\delta$, there will be a few particles moving out of the small islands every turn due to finite momentum aperture. These particles will not get lost at once provided $A_\delta \gg A_{\text{island}}$; furthermore, the existing rf system will help confine the particles not far away from the small islands boundary. Therefore most of particles will return to the small islands from outside under the effects of quantum fluctuation and radiation damping in the next few turns. As a result, an equilibrium beam distribution is established with permanent microbunched structure in phase space while individual particles are allowed to move out of and into the stable islands without loss. Now let us consider another effect, the single Coulomb scattering effect which is related to the Touschek lifetime. For the interested circumstances with small bucket height, especially the case that $A_{\text{island}}/\sigma_\delta$ is above and close to 3, the rate of particles moving out the small buckets due to single Coulomb scattering is usually much less than that due to finite momentum aperture, thus the equilibrium beam distribution varies little, corresponding to a long lifetime. On the other hand, in the case that $A_{\text{island}} < 3\sigma_\delta$, the number of particles moving out of the bucket from inside is larger than that of particles moving back from outside of the small islands every turn. Some particles will get lost at last, leading to a short lifetime.

As a brief summary of Sec. II, to realize the period-2 SSMB scheme for generating short microbunches, one should use modulation (rf or laser system) with normalized amplitude $K = eV_{\text{mod}}R_{56}k/E_0 > 4$. Increasing K, the relative bucket length R will be smaller, however, the relative bucket area S will decrease more rapidly due to the approximate relation $S \propto R^2$, implying less particles trapped in the small buckets. If K is so large that the bucket length $R\lambda_{\text{mod}} < \sigma_z$ and/or bucket height $A_{\text{island}} < 3\sigma_\delta$, the beam will have a short lifetime. As a compromise between the small bunch length and large enough particle trapping fraction, it is recommended to choose K slightly above 4 in a practical implementation of the period-2 SSMB.

III. SSMB FOR THZ COHERENT RADIATION IN SPEAR3 STORAGE RING

A. Period-2 SSMB using X-band rf system in SPEAR3 storage ring

As mentioned above, for the SSMB with a rf system, the modulation wavelength is relatively long, the momentum aperture is typically smaller than $\lambda_{\text{mod}}/\alpha C$, and only conventional buckets are allowed. However, in this situation, it is still possible to produce a sharply double-peaked longitudinal distribution by using the period-2 SSMB mechanism. For instance, with an X-band rf system, $\lambda_{\text{rf}} \sim 26$ mm, and equivalent harmonic $H = \lambda_{\text{rf}}/\Delta\lambda$ about 20, with $\Delta\lambda$ the separation of the two density peaks ~ 1 mm, the resulting coherent radiation wavelength λ_r is in the THz range. Thus, we can use an X-band cavity to establish microbunched beams in a storage ring for THz coherent radiation.

The main limitation of such a system is that the required modulation voltage of the X-band cavity is very high, for instance, $V_{\text{rf}} = E_0 K/e/R_{56}/k \approx 200$ MV with $K \approx 4.2$ for the 3 GeV SPEAR3 storage ring, provided that the X-band cavity is used in continuous operation mode (this limitation will be weaker for lower energy). As a compromise, we use the X-band cavity in pulse operation mode [20], modulating the beam once every multiple turns (to increase the equivalent R_{56} and reduce the required V_{rf}) with pulse duration of a fraction of turn instead of a full turn, so as to obtain a small duty factor and reduce the required voltage and power of the X-band cavity to an acceptable level.

We implement simulations of the period-2 SSMB in SPEAR3 storage ring based on the main parameters listed in Table II, while including radiation damping and quantum excitation effects (the application of the proposed SSMB mechanism is also explored for another storage ring at SLAC, the SLC damping ring [21], but will not be addressed here). In the simulation, a 3.7 m X-band rf cavity is placed in a 4.8 m long straight section of the SPEAR3 storage ring. The injection, trapping, and energy loss (due to synchrotron radiation) compensation are still supplied by the existing 476.3 MHz rf cavity. After the beam reaches an equilibrium state due to radiation damping and quantum excitation in several damping times, with rms bunch length $\sigma_z = 4.8$ mm and rms momentum spread $\sigma_\delta = 0.1\%$, the X-band rf cavity is turned on and provides voltage of 30.9 MV to the electron beam every eight turns (6.2 μs) with pulse duration of 1/5 turn (156 ns). The corresponding average power dissipated in the cavity is 20 kW/m, which is in a large but feasible level. (Nevertheless, the relatively high average power and high pulse repetition rate, 160 kHz, are still a challenge to rf scientists.) After tracking the beam for one million turns, the final beam distributions are shown in Fig. 7. About 27% of the particles survive and are microbunched to two short bunches with $\sigma_z \approx 0.3$ mm within each conventional bucket. We note that this bunch length is on the same order as that predicted by Eq. (2.39), $\sigma_z \approx 0.4$ mm. With appropriate R_{56} between the radiator (dipole) and the X-band cavity, we obtain a fixed density modulation structure at the radiator every eight turns, with the separation of double density peaks of 1.4 mm and bunching factor of 0.35. Our study shows that the particle loss mainly occurs in the first

TABLE II.   Main parameters of the period-2 SSMB scheme in the SPEAR3 storage ring.

Parameters	SPEAR3	Unit
Energy	3	GeV
Circumference	234.126	m
Nominal tune ν_x/ν_y	14.19/5.23	
Synchrotron tune ν_z (nominal/SSMB)	0.007/0.083	
Momentum compaction (nominal/SSMB)	0.0011/0.000 94	
Nominal rms bunch length	4.8	mm
rms energy spread	0.1	%
Revolution time, T_0	780.4	ns
Existing rf cavity, f	476.3	MHz
Existing rf cavity, V	3.2	MV
X-band rf cavity, f	11.4	GHz
X-band rf cavity, V	30.9	MV
X-band rf cavity, L	3.7	m
X-band rf cavity, pulse duration	1/5 (156)	Turns (ns)
X-band rf cavity, pulse interval	8 (6.2432)	Turns (μs)
X-band rf cavity, duty factor	0.025	
X-band rf cavity, aver. power	20	kW/m
X-band rf cavity, peak power	0.8	MW/m
X-band rf cavity, a/lambda	0.148	
Shunt impedance	91	M Ohm/m
Beam current/bunch	0.1	mA
No. particles/bunch	5×10^8	
Harmonic available	18	
Bunching factor, b	0.3	
Radiation wavelength	1.4	mm
Photon flux at dipole (bunches #)	$1.7 \times 10^{19}/8(50)$	Ph/[(sec)(0.1%BW)]
Brightness at dipole (bunches #)	$3.5 \times 10^{13}/8(50)$	Ph/[(mm)^2(mrad)^2(sec)(0.1%BW)]

several damping times after turning on the X-band cavity, and then, the beam reaches another equilibrium state with $A_{\text{island}}/\sigma_\delta \approx 3$ and particle loss due to the X-band modulation is negligible, corresponding to a long lifetime, as shown in Fig. 8. In addition, we test the sensitivity of the period-2 SSMB mechanism to various errors. It is found that such a scheme can tolerate relatively large modulation amplitude fluctuation, i.e., maximum $\Delta V/V = 5\%$, but small phase error, i.e., 0.05 degrees. An error in R_{56} mainly leads to a change to the separation between the two density peaks and, hence, the coherent radiation wavelength. However, this influence can be removed by installing a R_{56}-tunable chicane between the X-band rf cavity and the radiator. Unlike the very tight constraints from the transverse transfer elements, R_{51}, R_{52}, to the period-1 SSMB using laser modulation, the conditions of $R_{51}\sigma_x \ll \lambda_r$ and $R_{52}\sigma_{x'} \ll \lambda_r$ [6] turn out to be $R_{51}R_{52} \ll \lambda_r^2/\varepsilon_x \approx 60$ m with ε_x of 18 nm in this case, and can be easily satisfied, which implies the influence from the nonzero R_{51} and R_{52} is negligible for the proposed SSMB scheme in the SPEAR3 storage ring. The second-order dispersion T_{566} with amplitude up to $2R_{56}$ is tested in the simulation. The microbunching structure is not disturbed, only with little further particle loss, less than 0.5%. It appears the tolerance of higher-order dispersion is not very tight.

B. Limitation of the collective effects

Since the microbunched beam has a short bunch length, $\sigma_z \approx 0.3$ mm, short range wakefield (or high frequency impedance) will potentially lead to beam instability or severe heating at the locations of the devices which cause small discontinuities on the vacuum chamber.

The CSR wakefield is one of the dominant collective effects with short bunches. Theoretical and experimental studies show that bursts of coherent radiation will emerge when beam current is above the threshold of the CSR driven microwave instability [22,23]. A recent study taking into account the shielding effect [24] shows that with no shielding the particle distribution is deformed to have markedly triangular shape, and with increasing shielding the distribution profile moves gradually toward that of the unperturbed Gaussian. The threshold is given in the form

$$(S_{\text{csr}})_{\text{th}} = 0.5 + 0.12\Pi, \quad \text{with } (S_{\text{csr}})_{\text{th}} = N_{\text{th}}\frac{r_e\rho^{1/3}}{2\pi\nu_s\gamma\sigma_\delta\sigma_z^{4/3}},$$

$$\Pi = \frac{\sigma_z\rho^{1/2}}{h^{3/2}}, \tag{3.1}$$

where S_{csr} and Π are the dimensionless strength parameter and shielding parameter, respectively; r_e is the classical electron radius, N_{th} is the bunch population at the threshold,
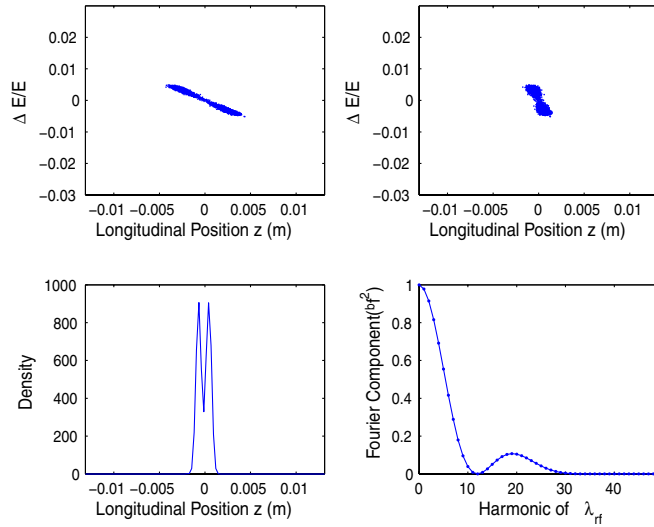
FIG. 7. SSMB in the SPEAR3 storage ring after 10^6 turns' tracking while including the existing 476.3 MHz rf cavity, radiation damping, and quantum excitation, with the beam distribution at the X-band rf cavity (top left), and the beam distribution (top right), density profile (bottom left) and Fourier component b_f^2 (bottom right) at the radiator, with b_f the bunching factor.

σ_z is the (zero current) rms bunch length, σ_δ is the nominal energy spread, and h is half of the separation between the two plates ($2h$ approximately corresponds to the vacuum chamber height).

From Eq. (3.1), for a given σ_z, N_{th} is proportional to the synchrotron tune ν_s. Note that $\nu_s \propto \alpha^{1/2}$ [25], thus we have $N_{th} \propto \alpha^{1/2}$. The traditional way to generate THz coherent
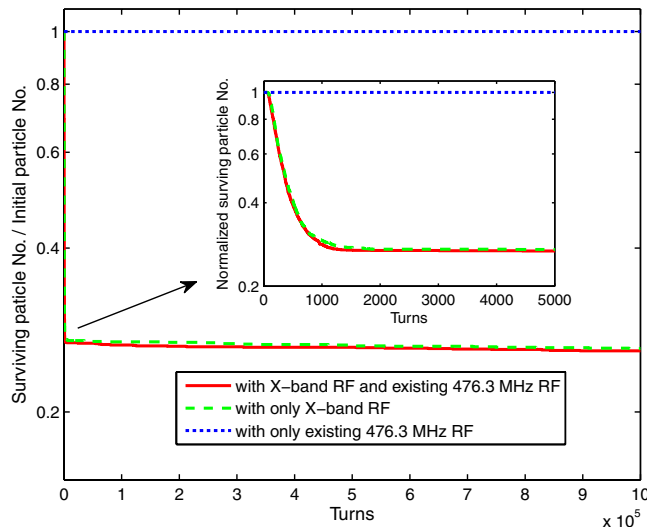

FIG. 8. Normalized surviving particles in the cases of with X-band rf and existing 476.3 MHz rf system (red solid), with only X-band rf (green dashed) and with only existing 476.3 MHz rf (blue dotted). The curves in the first 5000 turns are expanded on the image inset.

radiation in a storage ring is to reduce the bunch length to the submillimeter level by decreasing the momentum compaction α, i.e., using the "low α" mode. For the SPEAR3 storage ring, to obtain $\sigma_z = 0.3$ mm, it requires to reduce α to 1/256 of that of regular user operation optics. The available beam current for steady-state coherent radiation generation is quite limited. Equation (3.1) yields $N_{th} = 3.1 \times 10^7$ (beam current of $6\,\mu$A/bunch) for the SPEAR3 storage ring low α mode, which agrees well with the experimental scaling law for the bunch current limit $I(\mu\text{A/bunch}) = 5(\sigma_z/0.3\,[\text{mm}])^{2.354}$ [26]. In contrast, due to strong X-band modulation voltage and momentum compaction of the same order as that of regular user operation mode, the synchrotron tune of the period-2 SSMB is relatively large, $\nu_s = 0.083$, which results in a much higher threshold, $N_{th} = 6.0 \times 10^9$ (beam current of 1.2 mA/bunch).

In addition to the shielded CSR impedance, another strong source is the short range longitudinal wakefield associated with the small structure of the X-band rf cavity, which will cause the particles at the tail to lose more energy than that at the head of the bunch, and therefore introduce additional energy modulation to the particles and affect the final longitudinal distribution of the microbunched beams. We estimate the effect of the X-band cavity wakefield [27] by including it in the tracking simulation. Although the effect of asymmetrical energy loss within one bunch is partially alleviated by the relatively rapid synchrotron oscillation, the strong wakefield causes more particle loss, and limits the beam current to about 0.1 mA/bunch (5.0×10^8 electrons/bunch) with a bunching factor of 0.3. Note that this beam current is still much higher than that allowed by the low α mode of the SPEAR3 storage ring.

In the case of a short bunch, the heating from the interaction of the beam with small discontinuities (enlargements on the pipe) whose sizes are comparable to the short bunch length might become a serious problem for the performance of the storage ring. (The small X-band rf cavity structure will cause beam energy loss and local heating, which, however, can be moved by the designed cooling system for the rf cavity.) Thus, we consider an ideal case that there are $N_d = 100$ identical discontinuities more or less evenly distributed along the storage ring and estimate the heating power with the assumption of a single Gaussian distribution profile rather than the actual double-peak density modulation profile. The induced wake potential $W_\parallel$ is calculated with the code ECHO [28] and shown in Fig. 9.

The loss factor κ is [29]

$$\kappa = \int_0^\infty \frac{1}{\sqrt{2\pi}\sigma_z} e^{-z^2/2\sigma_z^2} W_\parallel(z)dz, \qquad (3.2)$$

which results in $\kappa \approx 0.5$ V/pC for one discontinuity.

For the stored beam of $N_b = 50$ bunches with 0.1 mA/bunch in the SPEAR3 storage ring, the average parasitic power is evaluated by
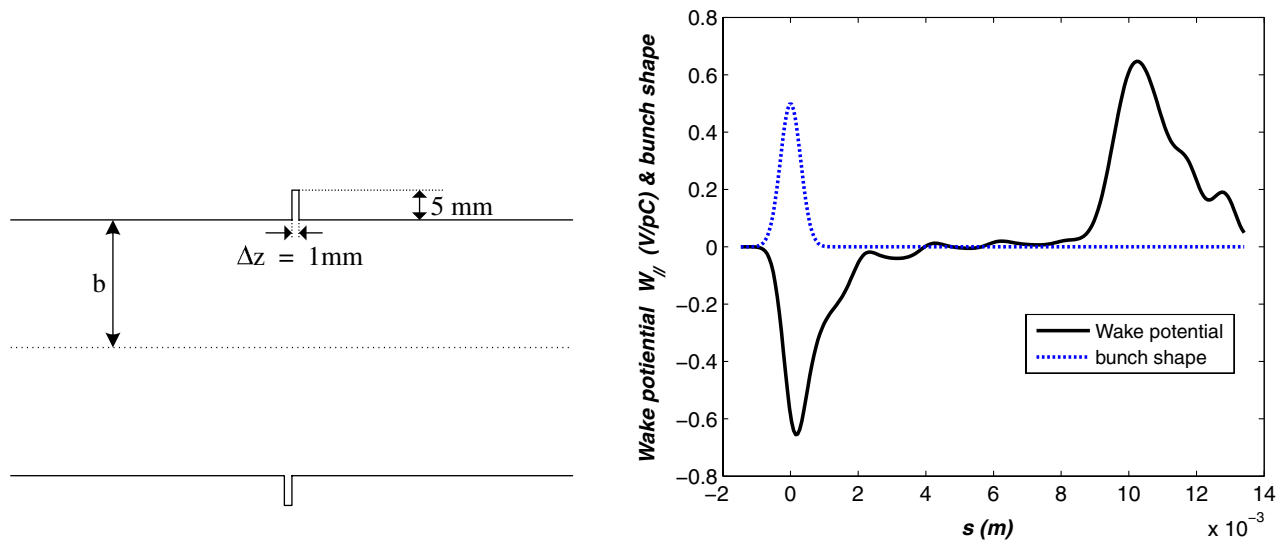
FIG. 9.   Model for one discontinuity on the perfectly conducting vacuum chamber (left) and wake potential calculated with ECHO code (right), $\Delta z = 1$ mm, $\Delta r = 5$ mm, and pipe radius $b \approx 17$ mm.

$$P_{\text{parasitic}} = \frac{q_b{}^2 N_d N_b \kappa}{T_0}, \qquad (3.3)$$

where q_b is the charge of a single bunch, $T_0 = C/c$ is the revolution time, with c being the speed of light. The resulting parasitic power is about 0.2 W per discontinuity and a total of 20 W, which is in an acceptable level.

C. Brilliance evaluation

Coherent radiation occurs when multiple electrons in a bunch radiate with a mutual relative phase, resulting in a quadratic dependence of the power on the number of participating electrons. For a given wavelength λ, the emitted average spectral power is given by

$$\frac{dP}{d\lambda} = N \frac{dp}{d\lambda}[1 + N b_f^2], \qquad (3.4)$$

where N is the number of electrons, b_f is the bunching factor, and $dp/d\lambda$ is the power from a single electron. The bunching factor b_f is defined by

$$b_f = \int e^{i2\pi z/\lambda} \rho_n(z) dz, \qquad (3.5)$$

where $\rho_n(z)$ is the normalized longitudinal density, satisfying $\int \rho_n(z) dz = 1$.

For the coherent radiation emitted from a dipole, $dp/d\lambda/d\psi$ is given by [30]

$$\frac{d^2 p}{d\lambda d\psi} = 2.7799 \times 10^{-16} \frac{E(\text{GeV})}{\lambda_r^2 C} S(\lambda_{cr}/\lambda_r), \qquad (3.6)$$

where $\lambda_{\text{cr}} = 4\pi\rho/3\gamma^3$ is the critical radiation wavelength, and $S(x) \approx 1.333 x^{1/3}$ for $x \ll 1$. For the SPEAR3 storage ring, the average radiation spectral power from a dipole is 1.6×10^{-15} W/m at the wavelength $\lambda_r = 1.4$ mm,

assuming the radiation in a deflection angle of $d\psi = 100$ mrad is collected.

Consider 50 bunches with 0.1 mA/bunch and bunching factor $b_f = 0.3$ stored in the storage ring. The total photon flux is

$$\text{flux} = \frac{(\frac{dP}{d\lambda})\lambda}{\hbar w} \times 0.1\% = 1.7 \times 10^{19} \text{ ph/[(sec)(0.1\%BW)]}. \qquad (3.7)$$

Since the microbunching structure is formed once every eight turns, the average photon flux of the coherent radiation is about $1.7 \times 10^{19}/8 \approx 2.1 \times 10^{18}$ ph/[(sec) × (0.1%BW)] and the brightness is about 4.4×10^{12} ph/[(mm)^2(mrad)^2(sec)(0.1%BW)], which is more than 1 order of magnitude higher than that produced by
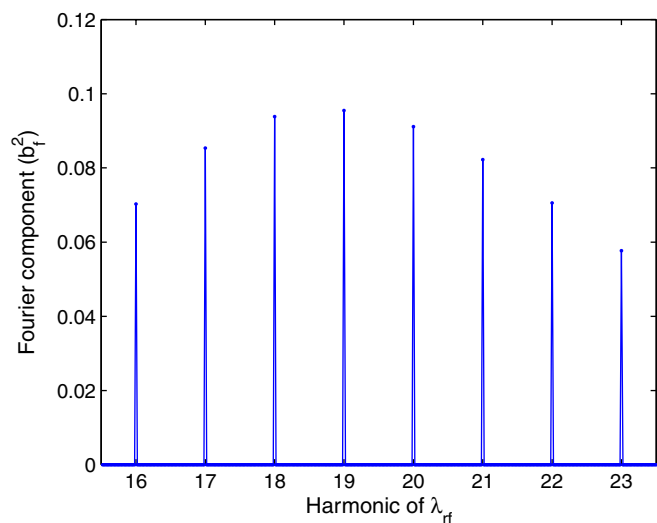

FIG. 10.   Square of the bunching factor b_f^2 at the radiator, with X-band rf cavity for both injection and modulation.

the low α mode in SPEAR3 storage ring of 280 bunches with 5 μA/bunch, with average photon flux about 1.7×10^{17} ph/[(sec)(0.1%BW)] [26].

D. *X*-band injection

Up to this point, we have assumed that the period-2 SSMB begins with injection using the existing 476.3 MHz rf system. As a result, the microbunch pairs are separated by the standard bunch spacing of about 0.6 m. Using the *X*-band rf cavity for both injection and modulation, we can store many more bunches in the storage ring, resulting in higher average beam current. More importantly, the regularly spaced microbunches exist over many periods, permitting bunching factors at only a narrow range of frequencies (see Fig. 10). The result is a sharper bandwidth and increased brightness of the THz coherent radiation.

IV. CONCLUSION

In this paper, we explore the dynamics of the SSMB system with a Hamiltonian and Jacobi matrix approach. Through the analysis, we reidentify the condition of the period-1 SSMB mechanism and propose the period-2 SSMB mechanism, which uses slightly stronger modulation but promises much smaller bunch length and, hence, higher harmonic than the period-1 SSMB mechanism. In addition, the proposed SSMB makes it possible to use an rf system instead of a laser system to produce microbunching. Taking the SPEAR3 storage ring as an example, we illustrate the application of period-2 SSMB to generate coherent THz coherent radiation using an *X*-band rf system in the pulse operation mode. Our study shows that the available beam current and the brightness produced by such a scheme can be much higher than that by a low α mode. For the SPEAR3 storage ring, the THz coherent radiation power enhancement is more than 1 order of magnitude. Throughout the paper, the transverse motion is assumed to remain stable in the presence of the proposed *X*-band rf modulation. This is a rather good assumption because the nonlinearities in transverse dimensions are relatively weak compared with the strong *X*-band sine function modulation and collective effects in the longitudinal plane, and the coupling between the transverse and longitudinal motions is usually weak in a typical storage ring. Nevertheless, a full 6D simulation is needed and will be implemented in the future.

ACKNOWLEDGMENTS

---

[1] J. Arthur *et al.*, Linac Coherent Light Source (LCLS) Design Study Report No. SLAC-R-521, 1998.

[2] K. J. Kim, Y. Shvydko, and S. Reiche, Phys. Rev. Lett. **100**, 244802 (2008).

[3] M. Tigner, Nuovo Cimento **37**, 1228 (1965).

[4] J. M. Klopf *et al.*, Nucl. Instrum. Methods Phys. Res., Sect. A **582**, 114 (2007).

[5] V. N. Litvinenko, S. F. Mikhailov, O. A. Shevchenko, and Y. Wu, in *Proceedings of the Particle Accelerator Conference, Chicago, IL, 2001* (IEEE, New York, 2001), p. 2619.

[6] Daniel F. Ratner and Alexander W. Chao, Phys. Rev. Lett. **105**, 154801 (2010).

[7] P. Bellomo *et al.*, SPEAR3 Design Report No. SLAC-R-609, 2002.

[8] M. Borland, Phys. Rev. ST Accel. Beams **8**, 074001 (2005).

[9] G. Decker *et al.*, Phys. Rev. ST Accel. Beams **9**, 120702 (2006).

[10] Y. Shoji *et al.*, in *Proceedings of the 10th European Particle Accelerator Conference, Edinburgh, Scotland, 2006* (EPS-AG, Edinburgh, Scotland, 2006), p. 163.

[11] A. Zholents, in *Proceedings of the 2007 Particle Accelerator Conference, Albuquerque, New Mexico* (IEEE, New York, 2007), p. 69.

[12] W. Guo, B. Yang, C.-x. Wang, K. Harkay, and M. Borland, Phys. Rev. ST Accel. Beams **10**, 020701 (2007).

[13] D. Xiang and G. Stupakov, Phys. Rev. ST Accel. Beams **12**, 080701 (2009).

[14] G. Wüstefeld, in *Proceedings of the 11th European Particle Accelerator Conference, Genoa, 2008* (EPS-AG, Genoa, Italy, 2008), p. 26.

[15] C. Biscari *et al.*, in *Proceedings of the 21st Particle Accelerator Conference, Knoxville, 2005* (IEEE, Piscataway, NJ, 2005), p. 336.

[16] J. Feikes *et al.*, in Proceedings of the 10th European Particle Accelerator Conference, Edinburgh, Scotland, 2006 (Ref. [10]), p. 157.

[17] B. V. Chirikov, Phys. Rep. **52**, 263 (1979).

[18] R. D. Ruth, Report No. SLAC-PUB-4103, 1986.

[19] B. V. Chirikov and F. M. Izraelev, in *Proceedings of the Colloques Internationaux du CNRS* (CNRS, Toulouse, 1973), p. 409.

[20] V. Dolgashev (private communication).

[21] N. Holtkamp (private communication).

[22] M. Venturini and R. Warnock, Phys. Rev. Lett. **89**, 224802 (2002).

[23] M. Venturini, R. Warnock, R. Ruth, and J. A. Ellison, Phys. Rev. ST Accel. Beams **8**, 014202 (2005).

[24] K. L. F. Bane, Y. Cai, and G. Stupakov, Phys. Rev. ST Accel. Beams **13**, 104402 (2010).

[25] H. Wiedemann, *Particle Accelerator Physics* (Springer-Verlag, Berlin, 1993), Chap. 8.1.2.

[26] X. Huang and J. A. Safranek (private communication).

[27] K. L. F. Bane, Report No. SLAC-PBU-9663, 2003.

[28] I. Zagorodnov and T. Weiland, Phys. Rev. ST Accel. Beams **8**, 042001 (2005).

[29] A. W. Chao, *Physics of Collective Beam Instabilities in High Energy Accelerators* (Wiley, New York, 1993), Chap. 2.

[30] A. W. Chao and M. Tigner, *Handbook of Accelerator Physics and Engineering* (World Scientific, Singapore, 2006), pp. 207–209.